

Giant electroresistance and tunable magnetoelectricity in a multiferroic junction

Francesco Ricci, Alessio Filippetti, and Vincenzo Fiorentini

CNR-IOM (UOS Cagliari) and Department of Physics, Cagliari University, 09100-Cagliari, Italy

(Received 2 September 2013; revised manuscript received 15 November 2013; published 13 December 2013)

First-principles density functional calculations show that the SrRuO₃/PbTiO₃/SrRuO₃ multiferroic junction with asymmetric (RuO₂/PbO and TiO₂/SrO) interfaces has a large ferroelectric depolarizing field, whose switching changes the interface transmission probabilities for tunneling electrons, leading to electroresistance modulation by over two orders of magnitude. The switching further affects the interface spin density, naturally driving magnetoresistance as well as modulated spin-dependent in-plane resistivity, which may be exploited in field-effect devices.

DOI: [10.1103/PhysRevB.88.235416](https://doi.org/10.1103/PhysRevB.88.235416)

PACS number(s): 73.40.-c, 75.70.-i, 77.80.Fm, 85.50.-n

I. INTRODUCTION AND METHOD

Multiferroic junctions are stacks of metallic ferromagnets and insulating ferroelectrics where electroresistance and magnetoresistance modulation^{1,2} have been obtained via polarization switching in the ferroelectric interlayer. Ferroelectric (FE) materials—especially perovskite oxides—are used as tunnel barriers between metal electrodes. Polarization charges accumulate at the interfaces of the finite FE layer with the rest of the stack, and cause a depolarizing field in the FE. Despite the strong screening by the metal electrodes, a sizable field survives in typical junctions. This persistence is the basis for nanoscale device concepts for data storage.^{3–5} A large (“writing”) external bias across the FE is used to switch the FE depolarizing field and polarization, and a small (“reading”) bias is then used to read the resistance of the stack in the newly realized state. This resistance may—in fact, in the present case, does—depend on polarization (i.e., depolarizing field) orientation, for instance because of interface structure or of asymmetries in potential profile along the junction and the associated tunneling probability. If that is the case, an electroresistance effect is realized.

When ferromagnetic electrodes are added to the junction, a multiferroic tunnel junction (MFTJ) is realized. Electron tunneling from the electrode through the FE barrier is now spin dependent, and the tunneling current also depends on the relative orientation of magnetization of the two electrodes, or on the local induced magnetization. Thus, in MFTJs, tunneling magneto- and electroresistance (TMR and TER) effects coexist, leading to four distinct states accessible via electric and magnetic external fields.^{6,7}

Further, because of the same asymmetries, the interface polarization charge is spin polarized to a degree depending on polarization direction. MFTJs may thus exhibit interfacial magnetoelectricity (ME), i.e., changes in interface magnetization induced by FE polarization reversal, hence ultimately driven by an electric field.^{8,9} The polarization switching changes sign and value of the FE charge at a given interface, but also its relative majority or minority spin content, establishing a tunable interface magnetization. Of course, this will affect both the tunneling (typically ballistic) and the in-plane (typically diffusive) transport in either spin channel.

In this paper, we study with first-principles calculations a SrRuO₃/PbTiO₃/SrRuO₃ (SRO/PTO/SRO) multiferroic tunnel junction, and specifically its tunneling electroresistance,

interfacial ME coupling, and in-plane transport. Due to the chemical asymmetry of the interfaces and the strong polarization of the FE layer, the electroresistance modulation is up to two orders of magnitude larger than in previous studies on BaTiO₃-based MFTJs.^{6,10} We also find a smaller but potentially useful tuning of in-plane resistance, originating from polarization-induced magnetization changes. Interface ME is present, with coupling coefficients similar to other MFTJs.¹¹

The electronic and atomic structure of the SRO/PTO/SRO junction is calculated within density functional theory in the generalized gradient approximation (GGA) and the projector augmented wave (PAW) as implemented in the VASP code.¹² PbTiO₃ (PTO) has been relaxed in tetragonal symmetry, obtaining $a = 3.924 \text{ \AA}$, $c = 4.176 \text{ \AA}$, Ti-O c -axis bonds 1.79 and 2.38 \AA , FE energy gain over paraelectric 108 meV, and polarization $P = 0.86 \text{ C/m}^2$. PTO cells with this structure and cubic SrRuO₃ (SRO) have been stacked keeping the in-plane lattice constant of PTO. The two interfaces between insulator and metal, RuO₂/PbO at one side and TiO₂/SrO at the other, are labeled “Ru” and “Ti” below and are simulated in an in-plane 2×2 section. The supercell has seven layers of PTO and six layers of SRO as short-circuited ferromagnetic electrode, for a total of 260 atoms. We consider the two ferroelectric states of PTO with polarization P pointing in opposite directions, perpendicular to the interfaces; all the quantities pertaining to P pointing from RuO₂/PbO to TiO₂/SrO (“Ru to Ti”) are depicted in blue, while those for P pointing from TiO₂/SrO to RuO₂/PbO (“Ti to Ru”) are in red. All configurations are reoptimized in length and relaxed with force tolerance 40 meV/\AA , using a $4 \times 4 \times 1$ k -point Monkhorst-Pack mesh.

II. RESULTS

A. Charge and potential

To analyze the total charge density (built adding narrow Gaussian charges at the ions location to the electronic charge) and electrostatic potential in the junction in the two polarization states, we feed their average over the sectional area $A = 4a^2$ of our 2×2 planar cell to a one-dimensional square-wave filter to obtain the macroscopic average¹³

$$\bar{n}(z) = \frac{1}{aA} \int_{z-a/2}^{z+a/2} dz' \int_A n(x, y, z') dx dy. \quad (1)$$

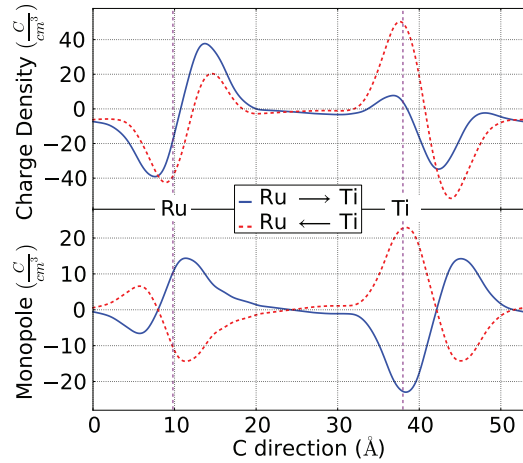


FIG. 1. (Color online) Macroscopic average (top) of the total charge density, and its monopole component (bottom) for the two directions of P in PTO.

Similarly to Ref. 14, we extract the monopole component of the macroscopically averaged density as

$$\frac{1}{2}[\bar{n}^{\rightarrow}(z - z_0) - \bar{n}^{\leftarrow}(z_0 - z)] \quad (2)$$

combining the density profiles \bar{n}^{\rightarrow} and \bar{n}^{\leftarrow} for the two P states (z_0 is chosen to minimize the monopoles and ends up near the midpoint of the FE layer).

The results are shown in Fig. 1. First, there is a significant net accumulation of charge at the two interfaces, due to the interface polarization discontinuity charge screened by the metal electrons and by the ionic response in both the insulator and the metal; the monopole is quite delocalized in comparison to that at semiconductor interfaces.¹⁴ This local charge produces a depolarizing field $E_{\text{dep}} \sim 5 \times 10^8$ V/m in the FE layer, which can be read off the potential profile in Fig. 2, as well as from the local density of states (Fig. 3) discussed below. For a finite polarized PTO slab of this thickness, the expected depolarizing field would be about 9×10^8 V/m assuming¹⁵ a static dielectric constant $\epsilon_s \sim 100$. The large residual field indicates that the metallic screening is incomplete, as suggested earlier.^{3,6}

Secondly, the asymmetric interfaces of highly polarized PTO produce quite different potential profiles for the two polarization directions, without any symmetry-breaking layer

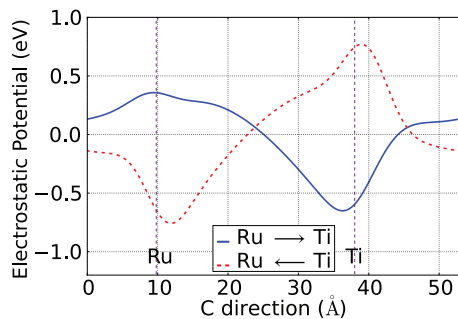


FIG. 2. (Color online) Asymmetric electrostatic potential profiles along c for opposite P 's in PTO. The depolarizing field is $\sim 5 \times 10^8$ V/m.

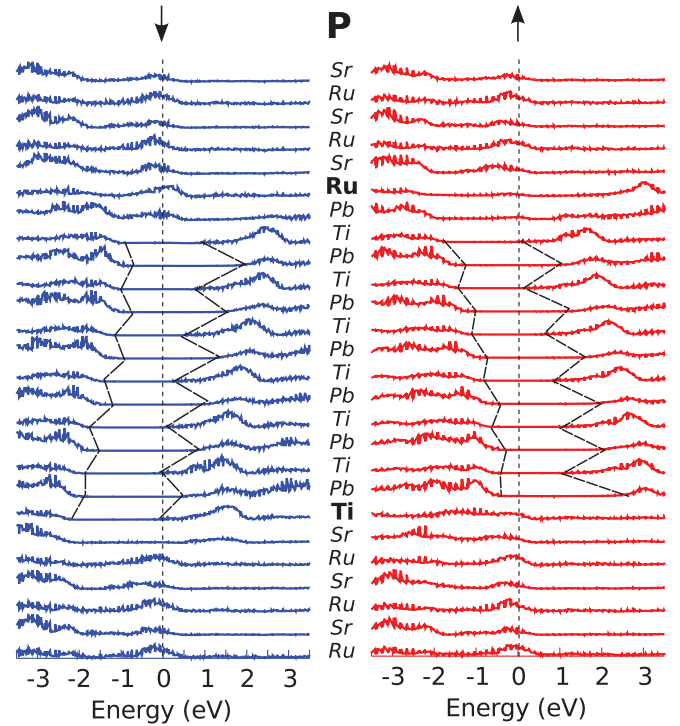


FIG. 3. (Color online) LDOS for the two polarization states.

of other materials interposed between the electrode and barrier.¹⁰ This implies that the tunneling resistance along the junction will be changed by the switching of PTO polarization. As suggested by simplified models,¹⁶ for such asymmetric potential and large residual electric field one expects a strong TER effect, which we now demonstrate calculating (a) the semiclassical tunneling conductance through the one-dimensional (1D) potential profile of the junction, and (b) the transmission coefficient from the evanescent-wave-function ratio in the insulator.

B. Tunneling electroresistance: WKB

To quantify the TER in our junction, we first study the semiclassical tunneling conductance through the 1D potential profile of the junction. An appropriate model for the potential profile through which the electrons tunnel is the position-dependent conduction band edge of the junction referred to as Fermi energy E_F . To extract this profile, we calculate for the two polarization orientations the layer-resolved local density of states (LDOS), which is displayed in Fig. 3. The position-dependent PTO band edges shift along the junction at a rate determined by the depolarizing field, whose value is in the mid 10^8 V/m as already indicated by the averaged potential profile. We then extract from the LDOS the position of the conduction edge in each layer, and use it to construct the potential profiles for the two values of P , which, as shown in Fig. 4, are strongly asymmetric.

We then calculate the tunneling probability in the semiclassical Wentzel-Kramers-Brillouin approximation through these two profiles vs injection energy, choosing the Fermi energy as zero. (This describes electrons tunneling into the PTO conduction band. Hole tunneling is neglected due to the

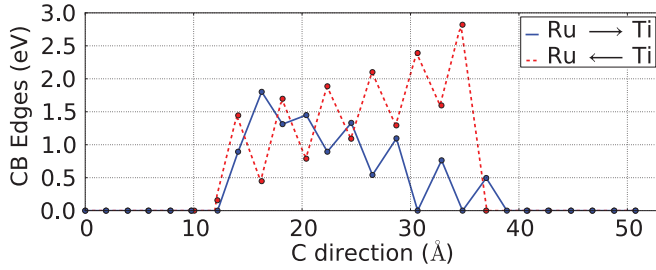


FIG. 4. (Color online) Conduction band (CB) edge potential profile for tunneling.

large barriers and effective masses.) As shown in Fig. 5 the ratio $G_{\rightarrow}/G_{\leftarrow}$, i.e., the TER, is between 50 and 350 depending on energy, and therefore up to two orders of magnitude larger than in BaTiO₃/SRO junctions.⁶ The absolute values of G are comparable with those found for similar junctions. We note that if we roughly estimate the writing voltage needed to reverse the depolarizing field in this structure as the field times the PTO thickness we find $Ed \sim 2$ V; thus, it would be safe to use a standard¹⁷ reading voltage of 0.5–0.6 V, which would yield a near-maximum TER.

C. Tunneling electroresistance: Transmission function

The second indication of a giant TER effect comes from the two transmission functions $T^{\rightarrow,\leftarrow}(\mathbf{k}_{\parallel})$ across the two interfaces in the two poling directions. For not too thin a barrier, the transmission function of a tunnel junction could be factorized¹⁸ as

$$\begin{aligned} T^{\rightarrow}(\mathbf{k}_{\parallel}) &= t_{\text{Ru}}^{\rightarrow}(\mathbf{k}_{\parallel}) \exp(-2\kappa(\mathbf{k}_{\parallel})d) t_{\text{Ti}}^{\rightarrow}(\mathbf{k}_{\parallel}), \\ T^{\leftarrow}(\mathbf{k}_{\parallel}) &= t_{\text{Ru}}^{\leftarrow}(\mathbf{k}_{\parallel}) \exp(-2\kappa(\mathbf{k}_{\parallel})d) t_{\text{Ti}}^{\leftarrow}(\mathbf{k}_{\parallel}), \end{aligned} \quad (3)$$

where d is the barrier thickness, $\kappa(\mathbf{k}_{\parallel})$ is the lowest decay rate in the barrier, and $t_{\text{Ru,Ti}}^{\rightarrow,\leftarrow}$ are the transmission probabilities from

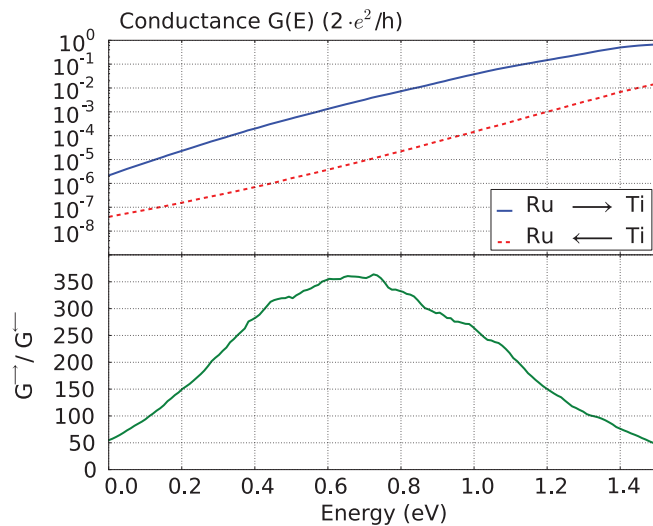


FIG. 5. (Color online) Top: conductance in the WKB approximation for tunneling through the 1D potential profiles shown in Fig. 4. Bottom: the TER between the two P states, topping at about 350.

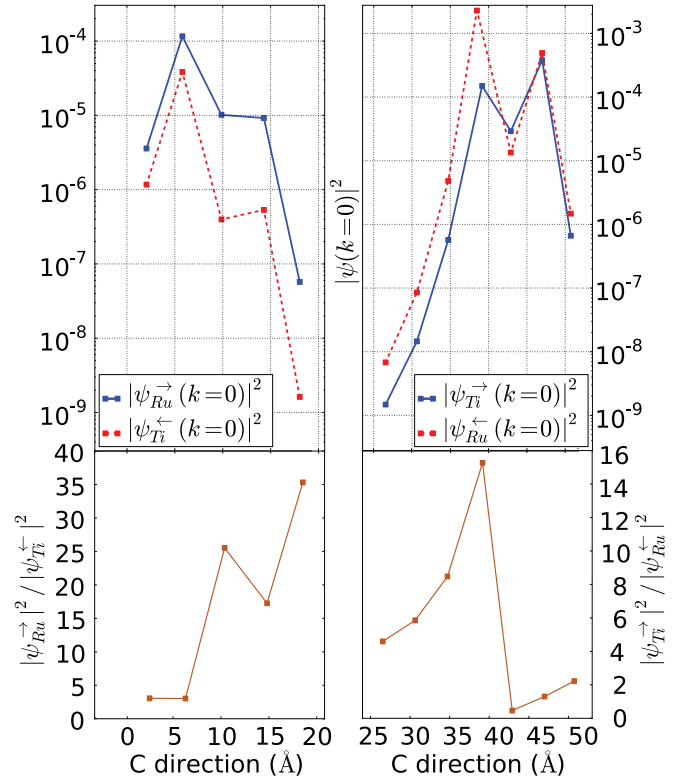


FIG. 6. (Color online) Probability densities at the Fermi energy and $\mathbf{k}_{\parallel} = 0$ (top) and their ratio (bottom) for the two polarization directions near the interfaces. Values taken at Ti sites

the left or right electrode into the barrier across the interfaces (Ru or Ti, respectively) for an electron with a given \mathbf{k}_{\parallel} , for both polarization directions.

In our junction, the two interfaces differ both chemically and electrostatically depending on the direction of polarization, hence we have four different t 's to assess. Assuming the same exponential decay for the two polarizations, we have

$$\frac{T^{\rightarrow}}{T^{\leftarrow}} = \left(\frac{t_{\text{Ru}}^{\rightarrow}}{t_{\text{Ti}}^{\rightarrow}} \right) \left(\frac{t_{\text{Ti}}^{\leftarrow}}{t_{\text{Ru}}^{\leftarrow}} \right). \quad (4)$$

The two t ratios can be extracted from the ratio of the density of metal-induced gap states at distance z from the two interfaces for the two poling directions, i.e.,

$$|\psi_{\text{Ru,Ti}}^{\rightarrow,\leftarrow}|^2 \propto t_{\text{Ru,Ti}}^{\rightarrow,\leftarrow}(\mathbf{k}_{\parallel}) \exp[-2\kappa(\mathbf{k}_{\parallel})z]. \quad (5)$$

The upper panels of Fig. 6 show the wave functions as a function of z for $\mathbf{k}_{\parallel} = 0$ at the Fermi energy along the junction for the two polarization directions, and the lower panels display their ratios. Thus, $t_{\text{Ru}}^{\rightarrow}/t_{\text{Ti}}^{\leftarrow} \sim 25$ and $t_{\text{Ti}}^{\rightarrow}/t_{\text{Ru}}^{\leftarrow} \sim 10$, so that the transmission ratio $T^{\rightarrow}/T^{\leftarrow}$ is about 250, a measure of the TER comfortably similar to the WKB result shown above.

D. Interface barriers and the origin of asymmetry

The asymmetry giving rise to the large TER is of electronic origin. This can be seen from the LDOS in Fig. 3: At the Ru-Sr-Ti interface (bottom right in Fig. 3), the PbO layer opposes a large barrier to tunneling, while the TiO₂ layer adjacent to SRO is metallized; at the Ru-Pb-Ti interface (top

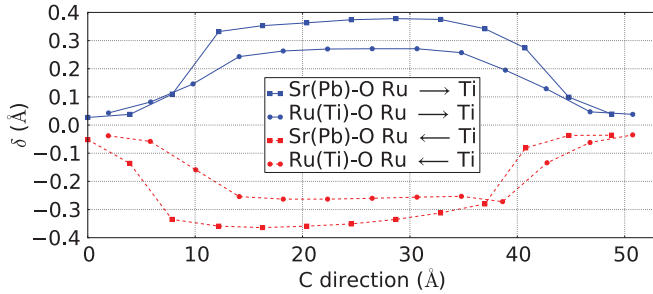


FIG. 7. (Color online) Cation displacement with respect to the plane of surrounding oxygens.

left in Fig. 3) the PbO layer in contact with SRO is metallized, and the first barrier is the smaller one provided by the TiO₂ layer. Put differently, the conduction Schottky barriers between SRO and PTO for the two interfaces are different; indeed, our estimated difference in the conduction edge position at the interface agrees with the calculated¹⁹ 0.7 eV difference between Schottky barriers of the two interfaces.²⁰ Since despite the gap underestimate in GGA this difference is well reproduced, both the TER and the absolute tunneling conductance should be considered quite accurate. We conclude that the smaller TER asymmetry in SRO/BaTiO₃ is related to its lesser or absent Schottky barrier asymmetry.²¹

Ionic screening, in turn, presents no significant surprise: Cationic displacements in the junction are rather well behaved, as shown by Fig. 7; they agree largely with previous estimates¹⁹ and are fairly similar to BTO/SRO (although here they are larger on average consistently with the larger polarization of PTO).

E. Interface magnetoelectricity

We now consider the interface ME effect. We elect to estimate the interface ME coefficient α assuming a linear magnetization-field relation

$$\mu_0 \Delta M = \alpha E. \quad (6)$$

Given the likely importance of nonlinearity for the high fields involved here, this should be considered an order-of-magnitude estimate. There is some latitude in deciding which magnetization changes are to be considered, depending on the operational procedure or application envisaged. In the present context, the natural scenario is polarization switching: ΔM is the integrated difference of magnetization density at each interface between the two polarization states. Clearly, two interface-related ME coefficients will result, either one of which will be relevant in practice depending on which interface is active in the specific experiment or application. To operationally implement this scenario, one just needs to switch P via the writing voltage.

To calculate the ΔM 's we define in analogy to the charge density in Sec. II A the macroscopic averages of the magnetization density $\overline{\vec{m}}^{\rightarrow}(z)$ and $\overline{\vec{m}}^{\leftarrow}(z)$ for the two states $\text{Ru} \rightarrow \text{Ti}$ and $\text{Ru} \leftarrow \text{Ti}$ of PTO polarization. In Fig. 8 we report the planar and macroscopic averages for the two P states. Upon switching, the magnetization changes strongly at the Ti interface, much less at the Ru one.

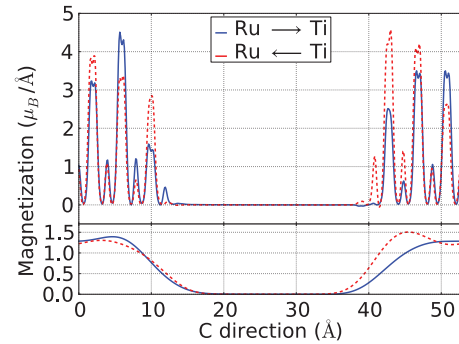


FIG. 8. (Color online) Planar and macroscopic averages of the magnetization in the two P states.

To calculate the α 's we conventionally choose the initial P state to be $\text{Ru} \rightarrow \text{Ti}$ and the final state $\text{Ru} \leftarrow \text{Ti}$. The magnetization changes at the Ru or Ti interface are

$$\begin{aligned} \Delta M_{\text{Ru}} &= \int_{\text{Ru}} (\overline{\vec{m}}^{\rightarrow} - \overline{\vec{m}}^{\leftarrow}) dz, \\ \Delta M_{\text{Ti}} &= \int_{\text{Ti}} (\overline{\vec{m}}^{\rightarrow} - \overline{\vec{m}}^{\leftarrow}) dz, \end{aligned} \quad (7)$$

where the integrals are done near each interface between the region of zero magnetization within PTO and the region of constant magnetization within SRO, specifically (see Fig. 8) between 2 and 21 Å for the Ru interface, and 31 and 49 Å for the Ti interface. We choose as electric field in Eq. (6) the depolarizing field E_{dep} , which is taken positive by convention (a different choice will simply change the sign of both ME coefficients). We then obtain the ME coefficients as

$$\alpha_{\text{Ru}} = \frac{\mu_0 \Delta M_{\text{Ru}}}{E_{\text{dep}}}, \quad \alpha_{\text{Ti}} = \frac{\mu_0 \Delta M_{\text{Ti}}}{E_{\text{dep}}}. \quad (8)$$

Table I summarizes the induced magnetizations [Eq. (7)] and the ME coefficients at the two interfaces [Eq. (8)]. Again the asymmetry in the interfaces shows up dramatically. The ME coefficients are somewhat smaller than those predicted for other similar MFTJs,^{9,11} despite our induced magnetizations being larger. This is due to our assuming conservatively a switching electric field larger than typical operational coercive fields of PTO. These may be 5–20 times smaller depending on external conditions and sample properties (and hence α could be larger by the same factors).

Some additional insight can be gained by examining in Fig. 9 the atom-resolved average magnetic moments obtained integrating the magnetization density within atomic spheres defined by the PAW construction. Consistently with its larger ME coefficient, the Ti interface (right side of each panel)

TABLE I. Magnetization changes (μ_B per interface cell) and ME coefficients (10^{-11} G cm²/V) upon switching P from $\text{Ru} \rightarrow \text{Ti}$ to $\text{Ru} \leftarrow \text{Ti}$.

Interface	ΔM	α
Ru	−0.31	−0.11
Ti	4.46	1.62

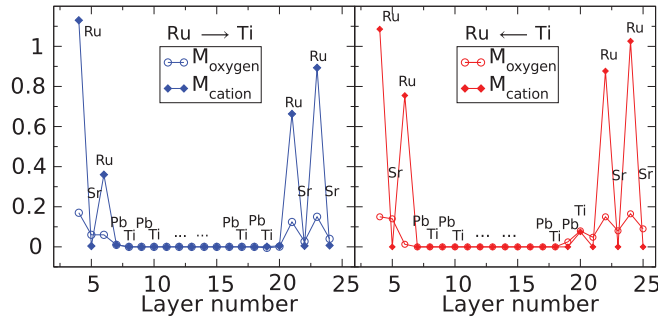


FIG. 9. (Color online) Atom-resolved magnetization (μ_B per atom) for the two polarization states (a few SRO layers omitted).

is more magnetically polarizable than the Ru interface. For $\text{Ru} \leftarrow \text{Ti}$ polarization (right panel), magnetization builds up in the first Ru layers, spilling over into the Ti metallized layer and through to the first insulating PbO layer. In $\text{Ru} \rightarrow \text{Ti}$ polarization (left panel), the interface Ru's lose some (and Ti and oxygens, all) of their moment. At the Ru interface (left side of each panel), the magnetization does not extend at all into PTO (specifically in the PbO layer) in either case, and the SRO magnetization mostly redistributes among Ru's and O's in the first and second layer, changing only slightly overall (see also Fig. 8).

In closing this section, we note that another possible choice for ΔM is the interface magnetization density change with respect to zero electric field.²² In our case, this translates into the magnetization difference at the two interfaces with or without the depolarizing field, i.e., for ferroelectrically distorted or paraelectric PTO. As P , i.e., the field, can be turned on in two ways, this procedure produces four ME coefficients $\alpha_{\text{Ru}}^{\rightarrow} \simeq \alpha_{\text{Ru}}^{\leftarrow} = 0.62$, $\alpha_{\text{Ti}}^{\rightarrow} = 0.14$, and $\alpha_{\text{Ti}}^{\leftarrow} = 1.75$, in units of $10^{-11} \text{ G cm}^2/\text{V}$. This polarization “turn-on” scenario, unfortunately, is essentially impracticable. It would require forcing PTO across its ferroelectric transition, e.g., by lowering the temperature across the Curie point T_c , with a small poling voltage applied to the junction to select the desired P state. This is largely incompatible with device operation due to the high $T_c \simeq 500^\circ\text{C}$.

F. In-plane conductivity modulation

The sizable interface asymmetry and ME coupling will influence the in-plane current in the SRO layer. To assess this effect, we use the BOLTZTRAP²³ code to calculate the conductivity in the plane of the junction in the diffusive regime as

$$\sigma_{\alpha\beta}(T; \mu) = \frac{1}{\Omega} \int \sigma_{\alpha\beta}(\epsilon) \left[-\frac{\partial f(T; \epsilon)}{\partial \epsilon} \right] d\epsilon \quad (9)$$

with

$$\sigma_{\alpha\beta}(\epsilon) = e^2 \sum_{i\mathbf{k}} \tau_{i,\mathbf{k}} v_{\alpha}(i, \mathbf{k}) v_{\beta}(i, \mathbf{k}), \quad (10)$$

where i is a band index, τ a relaxation time, v the group velocity calculated from the band structure, and f the occupation function. Assuming τ constant, we can plot σ/τ vs chemical potential. Although the scattering mechanisms may not be described in full detail, this approximation is quite sufficient

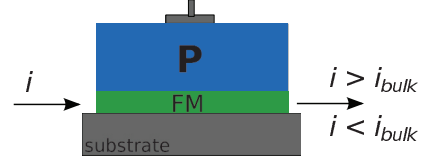
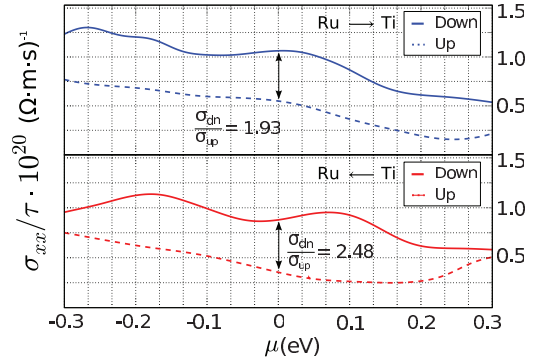


FIG. 10. (Color online) In-plane spin-resolved conductivity vs chemical potential for the two polarization states. Bottom: schematic device concept exploiting conductivity modulation.

to address conductivity ratios between polarization states. (We note in passing that diffusive conductivity is appropriate for in-plane transport, but may be inapplicable to tunneling transport depending on the nature of the Fermi surface of the junction system. In the present case this approach gives a $\text{TER} \sim 10^5$ which, while consistent with similar calculations for $1 + 6$ PTO/SRO superlattices,²⁴ is probably significantly overestimated.)

The in-plane spin-resolved conductivity in the diffusive regime in the two polarization states is shown in Fig. 10. The total conductivity changes by 35% upon polarization switching. Also, the switching modulates the down- to up-spin conduction ratio (2.5 to 1.9) by $\pm 15\%$ compared to the calculated bulk value (2.2). Such sizable modulations may be employed in in-plane field-effect devices such as that sketched in Fig. 10.

The electrically stored polarization orientation could be read electrically from the current modulation in the metal channel, i.e., effectively, as a modulated resistivity; this could be done either with the total current, or one of the spin components if polarized contacts are used. Another application of this configuration may be a filter or modulator of the incoming current, measuring the outgoing spin-polarized current calibrated to that of the bulk.

Note that our calculations measure the conduction within the whole PTO/SRO layer system, and there is no way to single out the net contribution of each interface; the exact values of the modulation will thus depend on SRO thickness, and will change if one of the interfaces (e.g., SRO/substrate) is “ferroelectrically dead.”

III. SUMMARY

In conclusion, we considered a multiferroic tunnel junction with asymmetric interfaces and a large-polarization FE. Very different potential profiles result for the two polarization states, and lead to a giant TER of up to 350. The interface

charge accumulation is spin polarized, with magnetization and magnetization changes depending on the interfaces and on polarization orientation, with sizable ME coefficients. The ME coupling affects the in-plane diffusive transport of the junction changing the majority to minority conductivity ratio, as well as the total conductivity. In particular, upon P inversion, the conductivity is modulated by 35% and its spin polarization by $\pm 15\%$, which is presumably exploitable in practical applications. In forthcoming work we plan to study

TMR, which may be expected to be high also, as well as the effects of magnetic doping of the FE layer.

ACKNOWLEDGMENTS

Work supported in part by MIUR-PRIN 2010 *Oxide*, IIT-Seed NEWDFESCM and POLYPHEMO, IIT “platform computation,” Fondazione Banco di Sardegna, and CINECA.

-
- ¹E. Y. Tsymbal, A. Gruverman, V. Garcia, M. Bibes, and A. Barthélémy, *MRS Bull.* **37**, 138 (2012).
²K. F. Wang, J.-M. Liu, and Z. F. Ren, *Adv. Phys.* **58**, 321 (2009).
³J. Junquera and P. Ghosez, *Nature (London)* **422**, 506 (2003).
⁴V. Garcia, S. Fusil, K. Bouzehouane, S. Enouz-Vedrenne, N. D. Mathur, A. Barthélémy, and M. Bibes, *Nature (London)* **460**, 81 (2009).
⁵A. Gruverman, D. Wu, H. Lu, Y. Wang, H. W. Jang, C. M. Folkman, M. Y. Zhuravlev, D. Felker, M. Rzechowski, C.-B. Eom, and E. Y. Tsymbal, *Nano Lett.* **9**, 3539 (2009).
⁶J. P. Velev, C.-G. Duan, J. D. Burton, Alexander Smogunov, M. K. Niranjan, E. Tosatti, S. S. Jaswal, and E. Y. Tsymbal, *Nano Lett.* **9**, 427 (2009).
⁷M. Y. Zhuravlev, S. Maekawa, and E. Y. Tsymbal, *Phys. Rev. B* **81**, 104419 (2010).
⁸C.-G. Duan, S. S. Jaswal, and E. Y. Tsymbal, *Phys. Rev. Lett.* **97**, 047201 (2006).
⁹C.-G. Duan, J. P. Velev, R. F. Sabirianov, Z. Zhu, J. Chu, S. S. Jaswal, and E. Y. Tsymbal, *Phys. Rev. Lett.* **101**, 137201 (2008).
¹⁰N. M. Caffrey, T. Archer, I. Rungger, and S. Sanvito, *Phys. Rev. Lett.* **109**, 226803 (2012).
¹¹M. K. Niranjan, J. D. Burton, J. P. Velev, C.-G. Duan, S. S. Jaswal, and E. Y. Tsymbal, *Appl. Phys. Lett.* **95**, 052501 (2009).
¹²G. Kresse and J. Furthmüller, *Phys. Rev. B* **54**, 11169 (1996); G. Kresse and D. Joubert, *ibid.* **59**, 1758 (1999).
¹³M. Peressi, N. Binggeli, and A. Baldereschi, *J. Phys. D: Appl. Phys.* **31**, 1273 (1998).
¹⁴F. Bernardini and V. Fiorentini, *Phys. Rev. B* **57**, R9427 (1998).
¹⁵W. Guo, D. Jin, W. Wei, and H. J. Marisa, *J. Appl. Phys.* **102**, 084104 (2008); Ø. Dahl, J. K. Grepstad, and T. Tybell, *ibid.* **103**, 114112 (2008).
¹⁶M. Y. Zhuravlev, R. F. Sabirianov, S. S. Jaswal, and E. Y. Tsymbal, *Phys. Rev. Lett.* **94**, 246802 (2005).
¹⁷A. Chanthbouala, A. Crassous, V. Garcia, K. Bouzehouane, S. Fusil, X. Moya, J. Allibe, B. Dlubak, J. Grollier, S. Xavier, C. Deranlot, A. Moshar, R. Proksch, N. D. Mathur, M. Bibes, and A. Barthélémy, *Nat. Nanotechnol.* **7**, 101 (2011).
¹⁸K. D. Belashchenko, E. Y. Tsymbal, M. van Schilfgaarde, D. A. Stewart, I. I. Oleinik, and S. S. Jaswal, *Phys. Rev. B* **69**, 174408 (2004).
¹⁹Y. Umeno, J. M. Albina, B. Meyer, and C. Elsässer, *Phys. Rev. B* **80**, 205122 (2009).
²⁰We obtain a similar value using the standard procedure of Ref. 13 for nonpolar PTO. The monopole component could not be completely eliminated from the potential profile in the polar case, leading to large uncertainties in the final value.
²¹P. Ghosez and J. Junquera, in *Handbook of Theoretical and Computational Nanotechnology*, edited by M. Rieth and W. Schommers (American Scientific Publishers, Valencia, USA, 2006), Chap. 134.
²²J. M. Rondinelli, M. Stengel, and N. Spaldin, *Nat. Nanotechnol.* **3**, 46 (2008).
²³G. K. H. Madsen and D. J. Singh, *Comput. Phys. Commun.* **175**, 67 (2006).
²⁴S. J. Callori, J. Gabel, D. Su, J. Sinsheimer, M. V. Fernandez-Serra, and M. Dawber, *Phys. Rev. Lett.* **109**, 067601 (2012).